Scientific Research Publishing

Open Journal of Geology, 2024, 14, 787-804
https://www.scirp.org/journal/ojg
ISSN Online: 2161-7589
ISSN Print: 2161-7570

Geochemistry of Micas from Issia Granite Complexe: A Marker of Geodynamic Evolution

Koffi Joseph Brou*, Alain Nicaise Kouamelan, Koffi Raoul Teha

Université Félix Houphouët-Boigny (UFHB), Abidjan, Côte d'Ivoire
Email: *broukoffijoseph1986@gmail.com, kouamelan02@gmail.com, rkteha@hotmail.fr

How to cite this paper: Brou, K.J., Kouamelan, A.N. and Teha, K.R. (2024) Geochemistry of Micas from Issia Granite Complexe: A Marker of Geodynamic Evolution. *Open Journal of Geology*, **14**, 787-804.
https://doi.org/10.4236/ojg.2024.148034

Received: July 23, 2024
Accepted: August 23, 2024
Published: August 26, 2024

Abstract

The granites and pegmatites located in the southern part of the Issia region, near the columbo-tantaliferous placers, are characterized by the presence of rare metals such as beryl, lithium and Nb-Ta oxides. They mainly consist of micas, quartz, plagioclase and potassium feldspar. The work carried out on the micas of these granites and pegmatites (EPMA analyses) has provided new geochemical data contributing to the understanding of the magmatic evolution of the Issia granite complex. Mineralogically, the most evolved G3 granites are characterized by their abundance of muscovite compared to biotite and the presence of pegmatite veins. Geochemically, the muscovites of the G1 and G2 granites are more ferriferous than those of the G3 granites, however, the latter display higher Na contents than the G2 and G3. The muscovites of the granites show an evolution from the pure muscovite series to the zinnwaldite series (micas of the pegmatites) which are lithium-bearing micas. The mineralogical and chemical data of the micas show that they are S-type peraluminous granites and demonstrate the formation of granites and pegmatites through fractional crystallization of the same parental magma.

Keywords

G3 Granites, Peraluminous Granites, Rare Metals, Fractional Crystallization

1. Introduction

The granitoids of the Paleoproterozoic domain have been the most studied in the West African craton. They appear in very varied aspects and have been described in turn as "magmatic", "migmatitic or metasomatic". Some authors thought that the granitoids reflected the composition of the rocks crossed during their emplacement [1]-[3]. The structuring (deformation) of these granitoids is more or less intense. The classifications proposed for these granitoids [4] take

into account their petrography and their structural context. In Ivory Coast, based on petrographic, geochemical and geochronological criteria, [5] [6] and [7] mainly distinguish: 1) granites with calc-alkaline affinity which show an Archean TTG type character and are dated around 2123 Ma; 2) late metaluminous to peraluminous granites dated around 2097 Ma. These are large batholiths of leucogranites (e.g. Ferkessédougou type) accompanied by small subcircular massifs of trondhjemites, pyroxene granites and alkaline granites (syenites and monzosyenites). The work of [8] in Guinea also shows that alkaline granites were emplaced at the end of the Paleoproterozoic. Geochronological data on the entire West African craton from [5] [7] [9]-[13] indicate that the emplacement of the Birimian granitoids was spread out during the Paleoproterozoic.

[14] showed that the coexistence of muscovite with biotite is a common mineralogical indicator of a highly peraluminous composition of plutonic rocks. Thus, the identification of primary muscovite is important because it is usually a good indicator of both magma composition and crystallization depth. With this group of common and relatively abundant minerals in the granites and granitic pegmatites of Issia [14], we can thus, with these different micas, provide the characteristics of the different stages of the evolution of the granitic complex of Issia.

In this article, we present a geochemical study of micas minerals from outcrops of G1, G2 and G3 granites [15], intragranitic pegmatites and pegmatite clusters observed in the Issia region, a granite complex linked to the presence of rare metals in the alluvial, colluvial and eluluvial placers. Our objective in this work is to assess the degree of evolution of the complex, with an emphasis on mica minerals.

2. Geological Setting

The Issia granite complex represents the southern part of the Ferkessedougou batholith and is located in west-central Ivory Coast. It is a large, elongated, multi-story plutonic batholith that extends 500 km from the Burkina Faso border in the northeast to the Sassandra-Cavally domain (SASCA) in the southwest of the Ivory Coast (**Figure 1**). The Ferké batholith is composed of a two-mica granite with aluminum-potassium chemistry. It is oriented NE direction, forming a linear structure 5 to 50 km wide (**Figure 1(A)**). The deformations affecting this batholith have been described by [16] and [15]. According to [15], the Issia granite complex can be subdivided into three major group: the G1, G2 and G3 granites. According to [15], G1 are two-mica granites with dominant biotite (**Figure 1(B)**), igneous or I type, calc-alkaline to weakly peraluminous with low phosphorus contents (0.07% - 0.16% wt% P_2O_5). They contain oxides as ilmenite, rutile and titanomagnetite. G2 and G3 are two-mica leucogranites with dominant muscovite (**Figure 1(B)**), type S therefore of metasedimentary origin, strongly peraluminous (ASI > 1.19) with intermediate phosphorus contents (0.2% - 0.5% P_2O_5) and accessory minerals such as Zn-rich ilmenite, rutile and apatite.

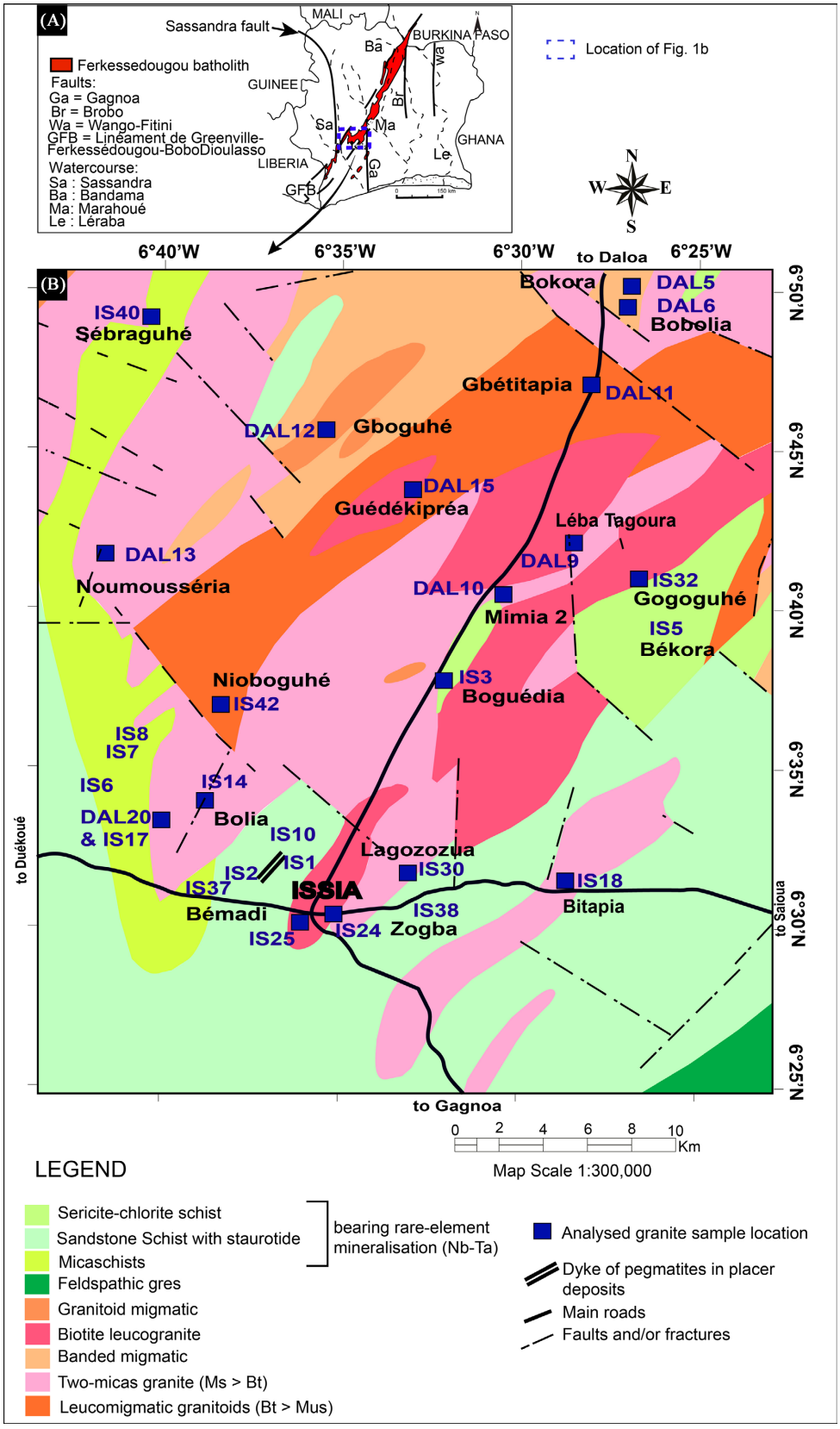

Figure 1. (A) Location of the Issia pluton in southern part of Ferké batholith. (B) Sampling points location on the simplified geological map of the study area. (Data provide [15]).

The G3 granites also have an abundance of tourmaline and are provided by pegmatite veins of varying thickness. The ilmenite of these granites is rich in Nb and Ta, and is sometimes associated with Nb-Ta oxides. These three groups of granites are also distinguished from each other by their rare earth spectra (REE) as well as their degree of differentiation. This is determined from classic differentiation parameters such as the Ba-Sr-Rb-Cs contents or the K/Rb and Nb/Ta ratios.

3. Analytical Method

Thin sections of different types of granites and pegmatites were studied under an optical microscope using transmitted and reflected light in order to characterize their textures and the different relationships between the mineral phases. The micas minerals were the subjected to in-situ geochemical analyzes for the major elements (microprobe) and trace elements (LA-ICPMS). These analyses provided insights into the evolution of the magmatic system and helped characterize the nature and origin of events, whether primary (*i.e.* magmatism) or secondary (*i.e.* hydrothermalism).

Major element analyzes were focused on several mineral species of micas including biotite and muscovite. The concentrations of major elements were obtained using a CAMECA SX Five electronic microprobe (EPMA) at the Raimond Castaing Microcharacterization Center of the Paul Sabatier University of Toulouse. The analysis was subjected with an accelerating voltage of 15 keV and an intensity of 10 nA, following the standard program Micas (MVL-Mica-Rb-Cs)-Silicates F-Cl-Ba dedicated to silicate minerals. The standards used were Albite (Na Ka), Rb Glass (Rb La), Al_2O_3 (Al Ka), Wollastonite (Si Ka, Ca Ka), Sanidine (K Ka), Cs Glass (Cs La), $MnTiO_3$ (Ti Ka, Mn), Fe_2O_3 (Fe Ka), Topaz-TR (F Ka), MgO (Mg), $BaSO_4$ (Ba La), Cr_2O_3 (Cr Ka), Graf (P Ka), SnO_2 (Sn La), Ta (Ta Ma), Tugtupite (Cl Ka), Cr_2O_3 (Cr Ka), Ni-G5 (Ni Ka). Since analyzes of mineral phases using a microprobe do not allow us to have the contents of trace elements such as Li, we used other techniques. The Li contents of the Issia (IS24, IS25), Liga (IS03), Bolia (IS14) massifs and the IS01 pegmatite observed in the metasediments were obtained using LA-ICP-MS (laser-ablation inductively coupled plasma-mass spectrometry) from the GET laboratory. For the other formations were calculated using the Tischendorf regression equations based on the ratios between Li_2O, F and Rb_2O with $Li_2O = 0.3935F^{1.326}$ ($R^2 = 0.843$, n = 199) [di 1] et $Li_2O = 1.579Rb_2O^{1.45}$ ($R^2 = 0.71$, n = 209) [di 2].

4. Results

4.1. Petrography Description of the Mica

The G1, G2 and G3 granites studied in the Issia region are generally two-mica granites with varying proportions [15] [17]. Biotite in granites G1, G2 and G3 represents proportions of 10 - 15 wt%, 8 - 12 wt% and 5 - 10 wt%, respectively. In the G1 and G2 granites, biotite is more or less chloritized, displaying a red-

dish-brown to greenish-brown color. In contrast the biotites observed in the G3 granites exhibit a brown to greenish brown color, sometimes appearing pale green, indicative of a fully chloritized biotite that have been replaced by muscovite. This biotite shows mineral stretching, with frequent zircon inclusion surrounded by pleochroic halos and traces of oxides marked by opaque spots. Muscovite is relatively scarce in the G1 and G2 granites compared to the G3 granites, represents 5 - 10 wt%, 8 - 15 wt% and 10 - 20 wt% respectively. Macroscopically, the muscovites in G2 granites have a silvery gray color. Under the microscope, they appear in different forms: either in the form of rods dispersed in the matrix and associated with quartz, plagioclase and microcline minerals or in flattened clusters replacing biotite. They can often be found as inclusions in plagioclase, quartz and microcline. Detailed petrographic descriptions and photomicrographs can be found in [15].

In intragranite pegmatites and non-granite pegmatites, most of the micas observed are muscovites. In intragranite pegmatites, fine-grained secondary muscovites are very often observed, replacing the feldspars and growing interstitially among the other minerals. At the granite-pegmatite contacts, muscovite appears very deformed, often found in folded bands and curved crystals, which are evidence of mechanical deformation. The primary muscovite in these pegmatites forms tabular crystals with medium to coarse grain sizes. In pegmatite outside of granite, muscovite occurs in small subautomorphic crystals associated with albite minerals, which are also very abundant. Incidentally, we observe minerals such as: apatite, ilmenite, tourmaline and Nb-Ta oxides.

4.2. Mineral Chemistry of Micas

4.2.1. Chemistry of Muscovite

The chemical composition of muscovites from three granite main group and micas for pegmatites is very varied (**Table 1** and **Table 2**).

Table 1. Chemical compositions and structural formulas of muscovites from Issia granitoids.

	Granites G1												Granites G2					
Locality	Ibobolia		Léba Tagoura		Gbétitapéa		Boguhé I		Noumousséria		Guédékipréa		Mimia II		Sébraguhé		Bitapia	
Muscovite	DAL05		DAL09		DAL11		DAL12		DAL13		DAL15		DAL10		IS40		IS18	
n	8		6		33		2		41		10		54		22		21	
	Mean	E-type	Mean	E-type	Mean	E-type	Mean	E-type	Mean	E-type	Mean	E-type	Mean	E-type	Mean	E-type	Mean	E-type
F	0.157	0.206	0.380	0.102	0.417	0.179	0.210	0.164	0.260	0.201	0.168	0.170	0.621	0.286	0.388	0.275		
Rb_2O	0.000	0.000	0.000	0.000	0.000	0.000	0.000	0.000	0.000	0.000	0.000	0.000	0.005	0.012	0.000	0.000	0.001	0.005
Al_2O3	29.110	2.495	28.898	1.520	32.646	0.342	31.680	0.440	31.735	1.891	31.182	0.452	32.260	0.751	33.829	0.686	33.291	0.478
SiO_2	46.044	0.997	44.035	1.820	46.154	0.603	45.930	0.634	45.762	1.200	46.163	0.608	47.067	0.916	47.056	0.403	46.164	0.312
K_2O	10.419	0.280	9.420	0.753	10.427	0.191	10.575	0.192	10.010	1.650	10.417	0.150	10.364	0.334	10.491	0.172	10.754	0.157
CaO	0.008	0.014	0.051	0.026	0.017	0.022	0.034	0.008	0.020	0.031	0.052	0.045	0.017	0.032	0.007	0.012	0.005	0.008

Continued

Cs_2O	0.008	0.011	0.010	0.012	0.014	0.013	0.016	0.018	0.009	0.014	0.010	0.017	0.009	0.018	0.012	0.012	0.015	0.024
TiO_2	1.362	1.019	1.074	0.231	0.512	0.029	1.055	0.117	0.641	0.129	0.982	0.202	1.024	0.179	0.988	0.189	0.642	0.188
MnO	0.023	0.026	0.030	0.020	0.033	0.027	0.025	0.023	0.048	0.061	0.033	0.039	0.033	0.028	0.034	0.028	0.020	0.021
FeO	5.176	0.721	4.100	0.663	3.694	0.126	4.095	0.030	4.581	2.085	4.445	0.117	3.204	0.194	2.205	0.157	1.978	0.190
Na_2O	0.167	0.084	0.271	0.037	0.302	0.053	0.206	0.049	0.274	0.090	0.281	0.049	0.303	0.083	0.324	0.074	0.369	0.070
MgO	1.492	0.515	1.288	0.145	0.827	0.096	0.995	0.023	0.960	0.576	1.015	0.104	1.169	0.174	0.875	0.157	0.835	0.115
BaO	0.029	0.033	0.055	0.044	0.032	0.033	0.015	0.005	0.009	0.015	0.029	0.018	0.013	0.022	0.023	0.027		
Cr_2O_3	0.005	0.009	0.015	0.017	0.015	0.020	0.000	0.000	0.017	0.026	0.027	0.030	0.022	0.026	0.029	0.032		
Li_2O													0.973	0.458			0.009	0.034
Sum	94	2.27	89.63	4.74	95.09	0.77	94.834	0.875	94.325	2.049	94.804	0.603	96.125	1.356	96.260	0.419	94.286	0.431
Al tot	4.741	0.356	4.910	0.071	5.242	0.069	5.196	0.002	5.143	0.237	5.013	0.080	5.073	0.089	5.293	0.104	5.315	0.066
Si ^{IV}	6.376	0.074	6.360	0.067	6.296	0.068	6.401	0.002	6.305	0.090	6.305	0.040	6.288	0.074	6.255	0.049	6.262	0.041
Al ^{IV}	1.624	0.074	1.640	0.067	1.704	0.068	1.599	0.002	1.695	0.090	1.695	0.040	1.712	0.074	1.745	0.049	1.738	0.041
Sum IV	8.000	0.000	8.000	0.000	8.000	0.000	8.000	0.000	8.000	0.000	8.000	0.000	8.000	0.000	8.000	0.000	8.000	0.000
Al ^{VI}	3.117	0.287	3.270	0.049	3.538	0.106	3.597	0.003	3.448	0.226	3.318	0.045	3.361	0.066	3.548	0.061	3.576	0.032
Ti	0.142	0.107	0.116	0.021	0.052	0.003	0.110	0.011	0.066	0.013	0.101	0.020	0.103	0.018	0.099	0.019	0.065	0.019
Fe^{2+}	0.599	0.088	0.492	0.058	0.320	0.182	0.003	0.003	0.422	0.355	0.507	0.013	0.358	0.024	0.245	0.018	0.224	0.022
Mn	0.003	0.003	0.004	0.002	0.004	0.003	0.003	0.003	0.006	0.008	0.004	0.005	0.004	0.003	0.004	0.003	0.002	0.002
Mg	0.309	0.109	0.278	0.042	0.168	0.019	0.206	0.002	0.199	0.129	0.206	0.021	0.233	0.035	0.173	0.031	0.169	0.024
Li*													0.513	0.240			0.082	0.000
SumVI	4.169	0.594	4.159	0.172	4.082	0.313	3.919	0.022	4.141	0.730	4.136	0.104	4.476	0.175	4.068	0.132	4.119	0.011
Na	0.045	0.022	0.076	0.010	0.080	0.014	0.055	0.013	0.073	0.024	0.074	0.013	0.078	0.021	0.083	0.019	0.097	0.018
K	1.838	0.028	1.731	0.068	1.812	0.035	1.878	0.060	1.753	0.279	1.813	0.037	1.764	0.068	1.777	0.030	1.858	0.029
Ca	0.001	0.002	0.008	0.004	0.002	0.003	0.005	0.001	0.003	0.005	0.008	0.007	0.002	0.005	0.001	0.002	0.001	0.001
Rb													0.001	0.002			0.000	0.000
Cs	0.000	0.001	0.001	0.001	0.001	0.001	0.001	0.001	0.001	0.001	0.001	0.001	0.000	0.001	0.001	0.001	0.001	0.001
SUM A	1.884	0.053	1.815	0.083	1.895	0.053	1.939	0.074	1.829	0.309	1.895	0.057	1.797	0.039	1.862	0.052	1.957	0.024

E-type: Standard deviation, n: number of analyses, Li*: Calculated Li.

Suite

Granites G3																		
Locality	Liga		Bolia				Issia centre				Lagozozua		Gogoguhé		Nioboguhé			
Musco-vite	IS03		IS14		IS17		IS24		IS25		IS30		IS32		IS42		IS42GF	
n	20		11		69		37		45		48		14		15		45	
	Mean	E-type	Mean	E-type	Mean	E-type	Mean	E-type	Mean	E-type	Mean	E-type	Mean	E-type	Mean	E-type	Mean	E-type
F					0.306	0.211			0.258	0.175	0.252	0.194	0.518	0.241	0.343	0.226	0.409	0.226

Continued

Rb_2O	0.016	0.025	0		0.006	0.017	0.003	0.009	0.002	0.010	0.002	0.006	0.004	0.009	0.005	0.017	0.010	0.021
Al_2O_3	32.018	0.516	34.012	0.266	33.852	0.838	33.897	0.373	33.642	0.745	34.614	0.420	33.419	0.512	34.072	0.430	34.090	0.479
SiO_2	46.018	0.350	46.027	0.217	46.231	1.148	45.922	0.350	46.034	0.688	47.030	0.960	46.353	0.529	46.984	0.864	47.154	0.639
K_2O	10.705	0.136	10.647	0.162	10.351	0.428	10.672	0.208	10.192	1.201	10.323	0.209	10.510	0.102	10.392	0.232	10.190	0.275
CaO	0.001	0.003	0.016	0.017	0.011	0.018	0.008	0.017	0.028	0.030	0.008	0.015	0.010	0.016	0.006	0.010	0.011	0.016
Cs_2O	0.033	0.042	0.022	0.025	0.028	0.039	0.020	0.030	0.020	0.025	0.033	0.044	0.040	0.041	0.029	0.043	0.029	0.040
TiO_2	0.962	0.131	0.547	0.051	0.575	0.152	0.473	0.094	0.393	0.136	0.472	0.121	0.509	0.177	0.663	0.221	0.152	0.017
MnO	0.036	0.031	0.015	0.028	0.019	0.022	0.015	0.019	0.036	0.029	0.029	0.022	0.022	0.025	0.028	0.019	0.069	0.031
FeO	2.731	0.141	1.636	0.107	1.957	0.171	1.674	0.155	2.349	1.072	2.172	0.141	2.813	0.301	2.124	0.127	2.788	0.301
Na_2O	0.349	0.051	0.435	0.108	0.373	0.087	0.414	0.064	0.379	0.110	0.381	0.053	0.355	0.093	0.384	0.082	0.337	0.071
MgO	0.961	0.106	0.668	0.039	0.930	0.117	0.670	0.054	0.736	0.112	0.859	0.070	0.886	0.090	0.984	0.076	0.717	0.064
BaO					0.012	0.017			0.020	0.021	0.003	0.009	0.010	0.020	0.020	0.031	0.002	0.007
Cr_2O_3					0.014	0.022			0.013	0.020	0.012	0.022	0.017	0.021	0.010	0.018	0.019	0.026
Li_2O	0.110	0.168	0.000	0.000	0.453	0.312	0.018	0.058	0.023	0.078	0.373	0.288	0.767	0.357	0.585	0.320	0.606	0.335
Sum	94.050	0.379	94.242	0.357	94.685	2.025	93.975	0.586	94.037	1.419	96.209	1.220	95.510	0.912	96.060	1.318	96.005	1.011
Al tot	5.152	0.078	5.419	0.029	5.345	0.085	5.417	0.047	5.376	0.065	5.377	0.067	5.252	0.077	5.307	0.039	5.310	0.066
Si ^{IV}	6.292	0.047	6.231	0.022	6.201	0.059	6.236	0.031	6.250	0.035	6.206	0.056	6.190	0.045	6.218	0.043	6.241	0.044
Al ^{IV}	1.708	0.047	1.769	0.022	1.799	0.059	1.764	0.031	1.750	0.035	1.794	0.056	1.810	0.045	1.782	0.043	1.759	0.044
Sum IV	8.000	0.000	8.000	0.000	8.000	0.000	8.000	0.000	8.000	0.000	8.000	0.000	8.000	0.000	8.000	0.000	8.000	0.000
Al ^{VI}	3.443	0.039	3.650	0.009	3.546	0.059	3.653	0.028	3.626	0.066	3.583	0.047	3.442	0.063	3.525	0.046	3.551	0.063
Ti	0.099	0.013	0.056	0.005	0.058	0.015	0.048	0.010	0.040	0.014	0.047	0.012	0.051	0.018	0.066	0.021	0.015	0.002
Fe^{2+}	0.312	0.016	0.185	0.012	0.219	0.018	0.190	0.017	0.267	0.128	0.239	0.015	0.314	0.033	0.235	0.017	0.308	0.033
Mn	0.004	0.004	0.002	0.003	0.002	0.003	0.002	0.002	0.004	0.003	0.003	0.002	0.002	0.003	0.003	0.002	0.008	0.003
Mg	0.196	0.022	0.135	0.008	0.186	0.023	0.135	0.011	0.149	0.024	0.169	0.013	0.176	0.018	0.194	0.016	0.141	0.013
Li*	0.055	0.000	0.055	0.000	0.244	0.167	0.109	0.001	0.164	0.001	0.197	0.152	0.410	0.189	0.309	0.167	0.322	0.178
SumVI	4.109	0.011	4.081	0.011	4.255	0.122	4.138	0.013	4.208	0.011	4.239	0.110	4.396	0.152	4.305	0.124	4.345	0.125
Na	0.092	0.013	0.114	0.028	0.097	0.023	0.109	0.017	0.100	0.029	0.097	0.013	0.092	0.025	0.098	0.020	0.086	0.018
K	1.864	0.025	1.836	0.032	1.769	0.069	1.846	0.037	1.761	0.201	1.736	0.045	1.788	0.021	1.753	0.052	1.718	0.042
Ca	0.000	0.000	0.002	0.002	0.002	0.003	0.001	0.002	0.004	0.004	0.001	0.002	0.001	0.002	0.001	0.001	0.002	0.002
Rb	0.001	0.002	0.000	0.000	0.000	0.001	0.000	0.001	0.000	0.001	0.000	0.000	0.000	0.001	0.000	0.001	0.001	0.002
Cs	0.002	0.002	0.001	0.001	0.001	0.002	0.001	0.002	0.001	0.001	0.001	0.002	0.002	0.002	0.001	0.002	0.002	0.002
SUM A	1.960	0.023	1.954	0.022	1.869	0.072	1.958	0.036	1.947	0.034	1.835	0.044	1.884	0.032	1.844	0.049	1.808	0.034

Table 2. Chemical compositions and structural formulas of muscovites and biotites from Issia pegmatites.

	Intragranitic pegmatites												Pegmatite intruvise sediments			
Locality	Bolia		Issia centre		Lagozozua		Gogoguhé		Nioboguhé				Gapoloroguhé			
Muscovite	IS17C2		IS25C		IS30P		IS32C		IS42P		IS42P1		IS01			
n	50		15		24		60		14		30		7		7	
	Mean	E-type	Mean	E-type	Mean	E-type	Mean	E-type	Mean	E-type	Mean	E-type	Mean	E-type	Moy	E-type
F	0.340	0.238	0.156	0.140	0.544	0.266	0.408	0.248	0.334	0.280	0.348	0.190				

Continued

Rb_2O	0.030	0.038	0.000	0.000	0.060	0.037	0.061	0.061	0.021	0.022	0.005	0.013	0.120	0.046	0.417	0.085
Al_2O_3	35.319	0.556	34.918	0.274	34.732	0.567	35.462	0.784	34.027	0.429	33.798	0.551	34.194	0.462	22.941	0.579
SiO_2	47.322	0.895	46.364	0.386	46.166	0.762	47.130	0.906	46.396	0.497	46.892	0.728	45.732	0.153	36.501	1.989
K_2O	10.323	0.272	10.297	0.363	10.296	0.231	10.130	0.630	10.396	0.227	10.597	0.147	10.350	0.205	8.394	0.322
CaO	0.013	0.019	0.006	0.011	0.011	0.017	0.015	0.018	0.010	0.015	0.008	0.014	0.040	0.050	0.022	0.024
Cs_2O	0.035	0.048	0.013	0.016	0.018	0.028	0.023	0.037	0.022	0.034	0.019	0.028	0.035	0.046	3.000	0.762
TiO_2	0.432	0.232	0.064	0.016	0.053	0.016	0.497	0.256	0.117	0.020	0.198	0.041	0.065	0.016	0.048	0.018
MnO	0.014	0.019	0.030	0.031	0.025	0.020	0.014	0.021	0.053	0.036	0.045	0.032	0.049	0.033	0.336	0.099
FeO	1.634	0.269	2.211	0.099	2.247	0.103	1.517	0.401	2.619	0.216	2.476	0.230	2.080	0.248	18.787	2.054
Na_2O	0.402	0.098	0.360	0.046	0.491	0.099	0.432	0.117	0.373	0.080	0.372	0.077	0.571	0.120	0.031	0.024
MgO	0.615	0.094	0.371	0.033	0.350	0.028	0.515	0.125	0.613	0.068	0.863	0.089	0.232	0.018	0.675	0.054
BaO	0.025	0.034	0.004	0.008	0.004	0.009	0.005	0.011	0.004	0.008	0.003	0.010				
Cr_2O_3	0.020	0.025	0.034	0.030	0.014	0.020	0.019	0.027	0.019	0.026	0.015	0.025				
Li_2O	0.504	0.353			0.807	0.394	0.605	0.368	0.496	0.415	0.516	0.282	0.809	0.310	2.511	0.141
Sum	96.558	1.499	94.828	0.448	95.053	1.495	96.261	1.514	95.044	0.779	95.664	0.858	93.738	0.442	91.291	0.305
Alt	5.446	0.068	5.519	0.033	5.456	0.040	5.473	0.117	5.367	0.071	5.295	0.093	5.526	0.047	5.526	0.047
Si^{IV}	6.199	0.039	6.227	0.021	6.161	0.033	6.179	0.057	6.217	0.045	6.241	0.056	6.272	0.033	6.272	0.033
Al^{IV}	1.801	0.039	1.773	0.021	1.839	0.033	1.821	0.057	1.783	0.045	1.759	0.056	1.728	0.033	1.728	0.033
Sum IV	8.000	0.000	8.000	0.000	8.000	0.000	8.000	0.000	8.000	0.000	8.000	0.000	8.000	0.000	8.000	0.000
	3.645	0.067	3.746	0.026	3.617	0.056	3.653	0.106	3.584	0.076	3.536	0.058	1.899	0.008	1.899	0.008
Ti	0.042	0.023	0.006	0.002	0.005	0.002	0.049	0.025	0.012	0.002	0.020	0.004	0.007	0.002	0.007	0.002
Fe^{2+}	0.179	0.031	0.248	0.011	0.250	0.013	0.166	0.043	0.293	0.024	0.275	0.026	0.107	0.013	0.107	0.013
Mn	0.002	0.002	0.003	0.004	0.003	0.002	0.002	0.002	0.006	0.004	0.005	0.004	0.006	0.004	0.006	0.004
Mg	0.120	0.019	0.074	0.007	0.070	0.006	0.101	0.024	0.122	0.013	0.171	0.018	0.048	0.004	0.048	0.004
Li*	0.263	0.182			0.431	0.208	0.318	0.192	0.265	0.221	0.275	0.150	0.110	0.001	0.110	0.001
SumVI	4.251	0.133	4.078	0.049	4.376	0.148	4.287	0.151	4.282	0.164	4.281	0.106	2.176	0.015	2.176	0.015
Na	0.102	0.025	0.094	0.012	0.127	0.025	0.110	0.029	0.097	0.021	0.096	0.020	0.152	0.031	0.152	0.031
K	1.723	0.038	1.762	0.068	1.751	0.035	1.692	0.104	1.775	0.038	1.797	0.031	1.811	0.043	1.811	0.043
Ca	0.002	0.003	0.001	0.002	0.002	0.002	0.002	0.003	0.001	0.002	0.001	0.002	0.000	0.000	0.000	0.000
Rb	0.002	0.003			0.005	0.003	0.004	0.005	0.002	0.002	0.000	0.001	0.011	0.004	0.011	0.004
Cs	0.002	0.003	0.001	0.001	0.001	0.002	0.001	0.002	0.001	0.002	0.001	0.002	0.002	0.003	0.002	0.003
SUM A	1.830	0.030	1.857	0.083	1.885	0.029	1.809	0.111	1.876	0.044	1.895	0.026	0.986	0.017	0.986	0.017

E-type: Standard deviation, n: number of analyses, Li*: Calculated Li.

Table 3. Chemical compositions and structural formulas of biotites from Issia granitoids.

	Granites G1												Granodiorite		Granites G2	
Locality	Ibobolia		Léba Tagoura		Gbétitapéa		Boguhé I		Noumousséria		Guédékipréa		Bokora		Sébraguhé	
Biotite	DAL05		DAL09		DAL11		DAL12		DAL13		DAL15		DAL06		IS40	
n	2		9		7		11		7		29		47		8	
	Mean	E-type	Mean	E-type	Mean	E-type	Mean	E-type	Mean	E-type	Mean	E-type	Mean	E-type	Mean	E-type
F	0.510	0.029	1.343	0.380	1.248	0.198	1.211	0.365	0.383	0.395	0.670	0.331	0.771	0.307	1.285	0.321
Rb_2O	0.000	0.000	0.000	0.000	0.000	0.000	0.000	0.000	0.000	0.000	0.000	0.000	0.000	0.000	0.000	0.000
Al_2O_3	15.783	0.607	16.132	0.858	17.664	0.238	16.990	0.281	18.968	2.254	16.038	0.351	15.598	0.360	18.072	1.526
SiO_2	34.820	1.172	34.551	1.563	34.675	0.190	35.505	0.495	37.022	1.844	34.948	0.579	37.635	0.567	35.641	1.027
K_2O	9.017	0.518	8.445	0.897	9.177	0.127	9.405	0.259	6.097	2.266	9.301	0.162	9.073	0.198	8.986	0.661
CaO	0.121	0.080	0.047	0.049	0.039	0.043	0.057	0.054	0.103	0.066	0.036	0.055	0.025	0.053	0.035	0.031
Cs_2O	0.000	0.000	0.017	0.023	0.016	0.017	0.006	0.009	0.012	0.017	0.009	0.015	0.007	0.012	0.025	0.028
TiO_2	2.793	0.175	2.589	0.293	2.343	0.087	2.681	0.200	1.022	1.021	2.678	0.208	1.909	0.136	2.782	0.250
MnO	0.351	0.016	0.244	0.067	0.697	0.066	0.337	0.113	0.404	0.183	0.508	0.058	0.193	0.043	0.299	0.059
FeO	20.139	1.009	18.021	2.888	23.730	0.205	19.526	0.666	20.185	2.915	22.320	0.411	13.412	0.248	22.830	1.995
Na_2O	0.002	0.003	0.037	0.028	0.038	0.032	0.042	0.026	0.099	0.055	0.053	0.032	0.108	0.031	0.057	0.030
MgO	8.225	0.148	6.557	0.310	5.352	0.268	9.023	0.260	5.373	0.839	7.930	0.253	14.914	0.325	5.698	0.459
BaO	0.005	0.007	0.051	0.038	0.003	0.006	0.049	0.036	0.002	0.005	0.027	0.031	0.686	0.053	0.033	0.023
Cr_2O_3	0.055	0.077	0.005	0.009	0.018	0.022	0.033	0.035	0.021	0.035	0.013	0.021	0.110	0.054	0.039	0.038
Li_2O																
Sum	91.817	3.592	88.038	6.915	95.000	0.652	94.865	1.222	89.691	3.878	94.532	0.936	94.441	1.099	95.780	0.831
Al tot	2.984	0.006	3.167	0.042	3.306	0.028	3.117	0.046	3.549	0.412	2.985	0.049	2.782	0.045	3.317	0.232
Si^{IV}	5.595	0.015	5.766	0.117	5.514	0.026	5.534	0.020	5.886	0.240	5.527	0.053	5.704	0.037	5.561	0.088
Al^{IV}	2.405	0.015	2.234	0.117	2.486	0.026	2.466	0.020	2.114	0.240	2.473	0.053	2.296	0.037	2.439	0.088
Sum IV	8.000	0.000	8.000	0.000	8.000	0.000	8.000	0.000	8.000	0.000	8.000	0.000	8.000	0.000	8.000	0.000
Al^{VI}	0.579	0.009	0.933	0.149	0.820	0.022	0.652	0.048	1.435	0.633	0.512	0.047	0.487	0.060	0.877	0.311
Ti	0.337	0.009	0.324	0.023	0.280	0.011	0.314	0.022	0.122	0.123	0.318	0.025	0.217	0.016	0.326	0.032
Fe^{2+}	2.701	0.037	2.495	0.256	3.151	0.037	2.541	0.076	2.681	0.393	2.948	0.055	1.698	0.033	2.978	0.290
Mn	0.048	0.004	0.034	0.009	0.094	0.009	0.044	0.015	0.055	0.025	0.068	0.008	0.025	0.005	0.040	0.008
Mg	1.968	0.036	1.629	0.061	1.267	0.058	2.094	0.071	1.272	0.200	1.867	0.062	3.365	0.077	1.325	0.119
Li*																
SumVI	5.633	0.095	5.415	0.498	5.611	0.136	5.645	0.232	5.566	1.375	5.712	0.197	5.791	0.192	5.546	0.760
Na	0.001	0.001	0.012	0.009	0.012	0.010	0.013	0.008	0.031	0.017	0.016	0.010	0.032	0.009	0.017	0.009
K	1.845	0.039	1.789	0.088	1.859	0.032	1.867	0.043	1.237	0.466	1.874	0.032	1.752	0.035	1.788	0.150
Ca	0.021	0.014	0.008	0.008	0.007	0.007	0.010	0.009	0.017	0.011	0.006	0.009	0.004	0.009	0.006	0.005
Rb																

Continued

Cs	0.000	0.000	0.001	0.002	0.001	0.001	0.000	0.001	0.001	0.001	0.001	0.001	0.000	0.001	0.002	0.002
SUM A	1.866	0.054	1.810	0.107	1.878	0.050	1.890	0.060	1.286	0.495	1.897	0.052	1.788	0.054	1.812	0.166
Mg/(Mg+Fe)	0.421	0.008	0.396	0.033	0.287	0.012	0.452	0.014	0.322	0.013	0.388	0.01	0.665	0.006	0.308	0.014

E-type: Standard deviation, n: number of analyses, Li*: Calculated Li.

G1 granites have FeO contents between 3.3 - 7.26 wt%, MgO = 0.77 - 2.82 wt%, TiO_2 = 0.46 - 2.92 wt%, Na_2O = 0.044 - 0.37 wt% and Al_2O_3 = 25.53 - 32.86 wt%.

G2 granites have contents of FeO = 1.96 - 3.2 wt%, MgO = 0.75 - 1.22 wt%, TiO_2 = 0.55 - 1.2 wt%, Na_2O = 0.31 - 0.42 wt% and Al_2O_3 = 31.88 - 34.56 wt%.

G3 granites have contents of FeO = 1.51 - 2.89 wt%, MgO = 0.6 - 0.97 wt%, TiO_2 = 0.33 - 1.06 wt%, Na_2O = 0.3 - 0.6 wt% and Al_2O_3 = 31.79 - 34.31 wt%.

To show the extent of phengitic substitution, we used the binary diagram R^{3+} versus Fe + Mg + Ti + (Si-3) ([18]; **Figures 2(A)-(C)**). In this diagram, we see that the muscovites align along the celadonite-phengite-muscovite line.

These muscovites, plotted in the ternary diagram Al_2O_3-K_2O-(MgO + FeO) of [19] (**Figure 2(E)**) show that this substitution takes place exclusively according to an arrangement between the muscovite and celadonite pole. The muscovites of the G1 and G2 granites are those which are closer to the celadonite pole.

When plotted in the classification diagram of [20] (**Figure 2(F)**), some muscovites from the IS25 granite of the G3 granite series fall into the field of iron-bearing muscovites. Similarly, some muscovites from the DAL13 and DAL05 granites of the G1 granite series show this iron-bearing character. However, most of the muscovite minerals analyzed fall into the range corresponding to pure muscovites. In the Ti-Na-Mg ternary diagram of [21], which distinguishes primary muscovites (magmatic muscovites) from secondary muscovites (muscovites resulting from alteration or late-magmatic) (Figures 2(G)-(I)), these iron-bearing muscovites fall into the field of secondary muscovites. Most muscovites from the G1 and G2 granites fall into the field of primary muscovites and show enrichment in Mg relative to Na and Ti (**Figure 2(H)**). In this ternary diagram, all muscovites of the IS42GF granite fall into the field of secondary muscovites (**Figure 2(I)**) and display an evolutionary trend from the Mg pole to the Na pole. The muscovites of the intragranitic pegmatites IS42P and IS42P1, which cut the IS42GF granite, present the same characteristics as the latter (**Figure 2(G)**). The muscovites of intragranitic pegmatites IS17C2, IS32C and IS30P, although secondary, also evolve towards the Na pole. The IS17C2 and IS32C thin sections made at the granite-pegmatite contact show that the muscovites richest in Na are those located at the boundary or in the pegmatite. In the ternary diagram of [21], it is evident that all the muscovites of the granitic pegmatites evolve towards those of the muscovites of the extra-granitic pegmatite (IS01) by becoming enriched in Na (**Figure 2(G)**).

The different dioctahedral micas thus analyzed were plotted in the binary

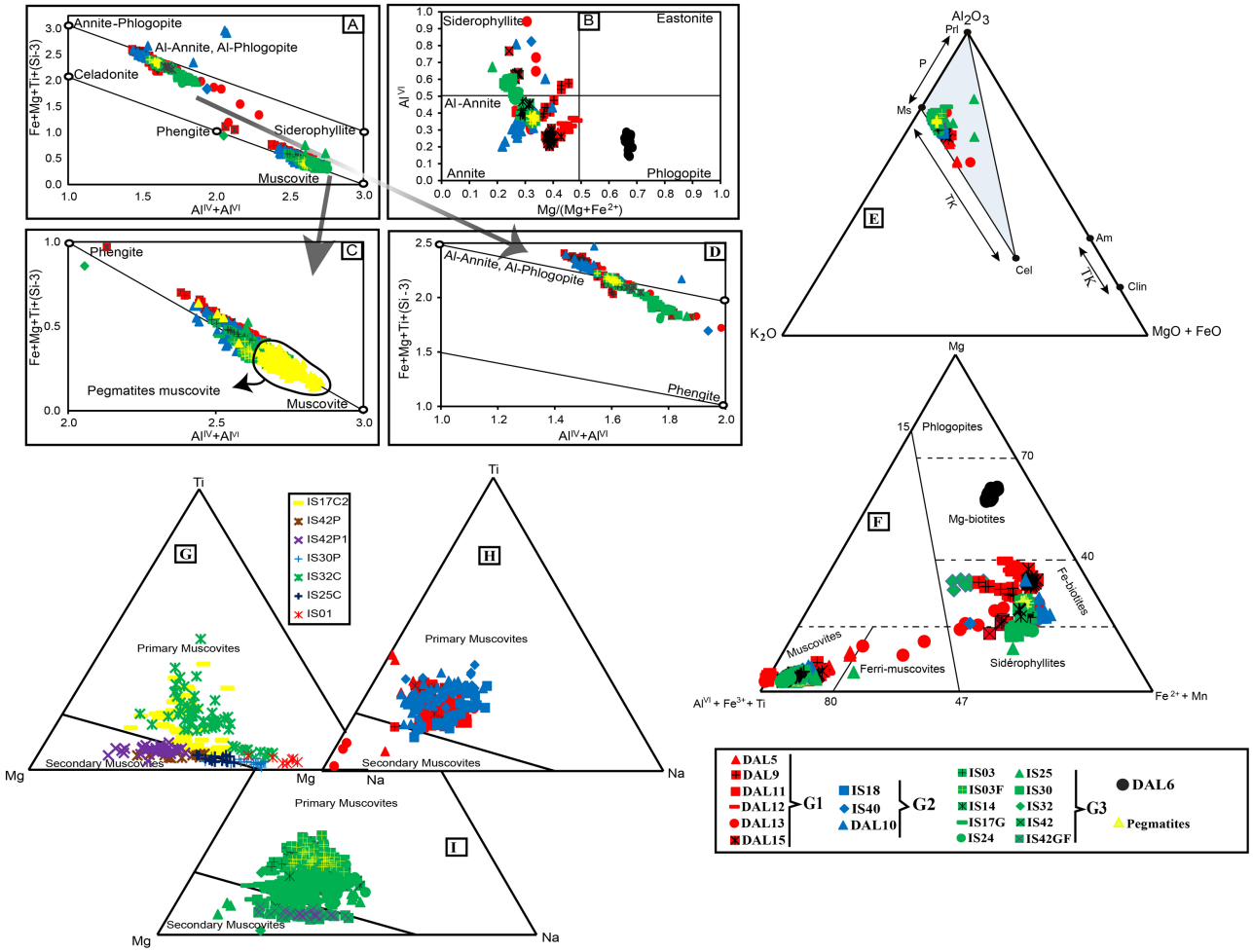

Figure 2. (A)-(D) Chemical composition of dioctahedral and trioctahedral micas from granites and pegmatites of the Issia region in the [18] diagram. Values are in atoms per formula unit (a.p.f.u). (A) Dioctahedral and trioctahedral micas in the Fe + Mg + Ti+ (Si-3) diagram as a function of Al^{IV} + Al^{VI}, (B) Position of trioctahedral micas in the Al^{VI} diagram as a function of Mg/(Mg + Fe), (C) Distribution of dioctahedral micas on the phengite-muscovite segment, (D) Distribution of trioctahedral micas on the Al segment. Annite, Al. Phlogopite-siderophyllite. (E) Chemical compositions of muscovites from granites of the study area represented in the ternary diagram Al_2O_3-K_2O-(MgO + FeO) of [19] showing a Tschermak substitution. (F) Classification of micas (biotites, muscovites) in the ternary diagram Mg-Al^{VI} + Fe^{3+} + Ti-Fe^{2+}+ Mn according to [20]. (G)-(I) Chemical compositions of muscovites represented in the Ti-Na-Mg ternary diagram of [21]. (G) Muscovites of pegmatites. (H) Muscovites of granites G1 et G2. (I) Muscovites of granites G3.

diagram of [22] which has the axis variation [Fe_{tot} + Ti+ Mn − Al^{VI}] as a function of [Mg-Li]. In this diagram, the compositions of the micas fall into the quadrants of the muscovite-Li-muscovite-phengite-Li-phengite series (**Figure 3(A)** & **Figure 3(B)**). This reflects their alignment on the Phengite-Muscovite segment defined by the [18] diagram. The micas of pegmatite IS01 fall into the field of zinnwaldite, thus expressing their enrichment in Li. In **Figure 3(B)**, we observe an enrichment in Fe of the micas, that is to say an evolution from the muscovite group towards the zinnwaldites group which are lithiniferous micas.

4.2.2. Chemistry of Biotite

The chemical compositions of the biotites from the different granite facies analyzed

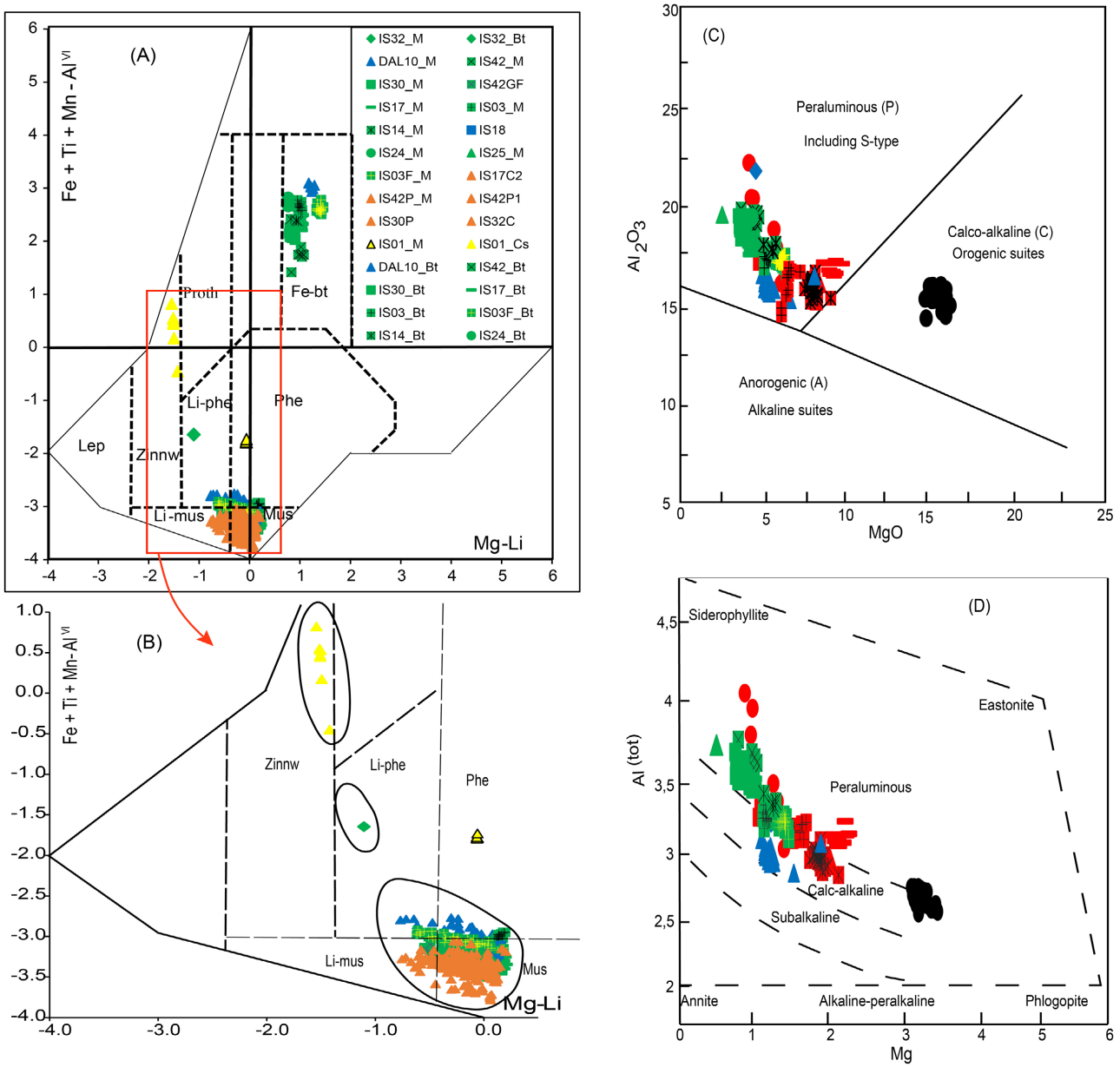

Figure 3. (A) Position of trioctahedral and dioctahedral micas from Issia granites and pegmatites in the diagram Y (Fe + Mn + Ti-Al^{IV}) as a function of Mg-Li (modified by [22]). (B) Evolution from the Al-rich micas pole to the Fe-rich micas pole. Mus: Muscovite, Fe-bt: Fe-biotite, Li-phe: Li Phengite, lipid: Lepidolite, Zinnw: Zinnwaldite, proth: Protholitionite. (C), (D) Diagrams showing magma types from the chemical composition of biotites. (C) Position of biotites in different magmatic lineages in the Al_2O_3 diagram as a function of MgO after [23] [24]; with P = biotite from peraluminous suites (S-type granites), A = biotite from alkaline anorogenic suites and C = biotite from calc-alkaline orogenic suites. B = Al (tot) classification diagram as a function of Mg from [25]. The legend of C and D is the same as that of **Figure 2**.

are recorded in **Table 3**. Chemically, they are iron-bearing biotites ($0.52 < XFe < 0.73$ for G1 granites; $0.61 < XFe < 0.73$ for G2 granites and $0.66 < XFe < 0.82$ for G3 granites) with XFe = Fe/(Fe + Mg). as Additionally, the exhibit high contents of Al^{IV} (1.94 - 2.51 for G1; 2.25 - 2.49 for G2 and 2.3 - 2.6 for G3) and Ti (0.12 - 0.34 for G1; 0.28 - 0.33 for G2 and 0.22 0.34 for G3). The biotites of the G1 granites, located in the northern part of the Issia region are slightly more magnesian

and less iron-bearing than those of the G3 and G2 granites (**Figures 2(B)-(F)**). Apart from the biotites of the granites, those of the Bokora granodiorite (DAL06) are magnesian with XMg located between 0.66 - 0.68 (XMg = Mg/(Mg + Fe)).

In the MgO versus Al_2O_3 diagram proposed by [23] [24] to discriminate biotites from alkaline magma (A), peraluminous magma (P) (type S) and calc-alkaline magma (C), the biotites from the Issia granites fall into the field of peraluminous granites (P) (**Figure 3(C)**). These biotites are highly aluminous (15.02 - 21.82 wt% Al_2O_3), which therefore coincides with the aluminum saturation index of the granites (1.14 - 1.51).

In the classification diagram using the Al (tot) versus Mg parameters of [25] (**Figure 3(D)**), the biotites of the G3 granites almost all fall into the field of peraluminous magmas, for except of the biotites of the IS03f and IS03 granites, which are located at the boundary peraluminous and calcalkaline magmas. All the biotites of the G2 granites are positioned in the field of calc-alkaline magmas. The biotites of the G1 granites are distributed in the fields of both calcalkaline and peraluminous magmas. The granodiorite biotites display a calc-alkaline magma character. In this diagram, a decrease in Al in biotites is accompanied by an increase in Mg.

In the diagram by [18] (**Figures 2(A)-(D)**), which illustrates the occupation of the octahedral site (Fe + Mg + Ti + (Si-3)) as a function of the Al_{total}, all of the trioctahedral micas of the different granites are located along the annite-phlogopite-siderophyllite joint, near the Al-annite-Al-phlogopite pole.

In the Al^{VI} versus Mg/(Mg + Fe^{2+}) diagram [18] (**Figure 2(B)**), we observe that all the biotites correspond to Al-annites s.l. and we see good discrimination of the different compositions. In this diagram, the biotites of G3 granites show an evolution from the Annite-phlogopite pole towards the Siderophyllite pole, indicanting a constant increase in Fe compared to Mg and, therefore, a substitution of Al^{VI} by Fe^{2+} compared to Mg^{2+}. On the other hand, the biotites of the G1 and G2 granites evolve preferentially from the Annite pole towards the Eastonite pole, which indicates a substitution of Al^{VI} by Mg^{2+} compared to Fe^{2+}. Alignment of granodiorite biotite analysis points shows an increase in Al during magma evolution with almost constant XMg.

To discriminate between primary biotites, rebalanced primary biotites and secondary biotites, the analysis data were inserted into the ternary diagram 10*TiO_2-MgO-FeO + MnO of [26] (**Figure 4**). In this diagram, we notice that the majority of analysis points for G1 granites are found in the field of primary biotites, though sometimes at the limit and in the field of chemically rebalanced biotites. We also observe two (02) points of the DAL13 granite in the secondary biotite field (**Figure 4(A)**). The biotites of G2 granites are generally located in the field of primary biotites. However, we can observe a point in the domain of reequilibrated biotites and another in that of secondary biotites (**Figure 4(B)**). Finally, concerning the biotites of the G3 granites, they are all in the field of primary biotites but sometimes close to the limit of rebalanced biotites (**Figure 4(C)**).

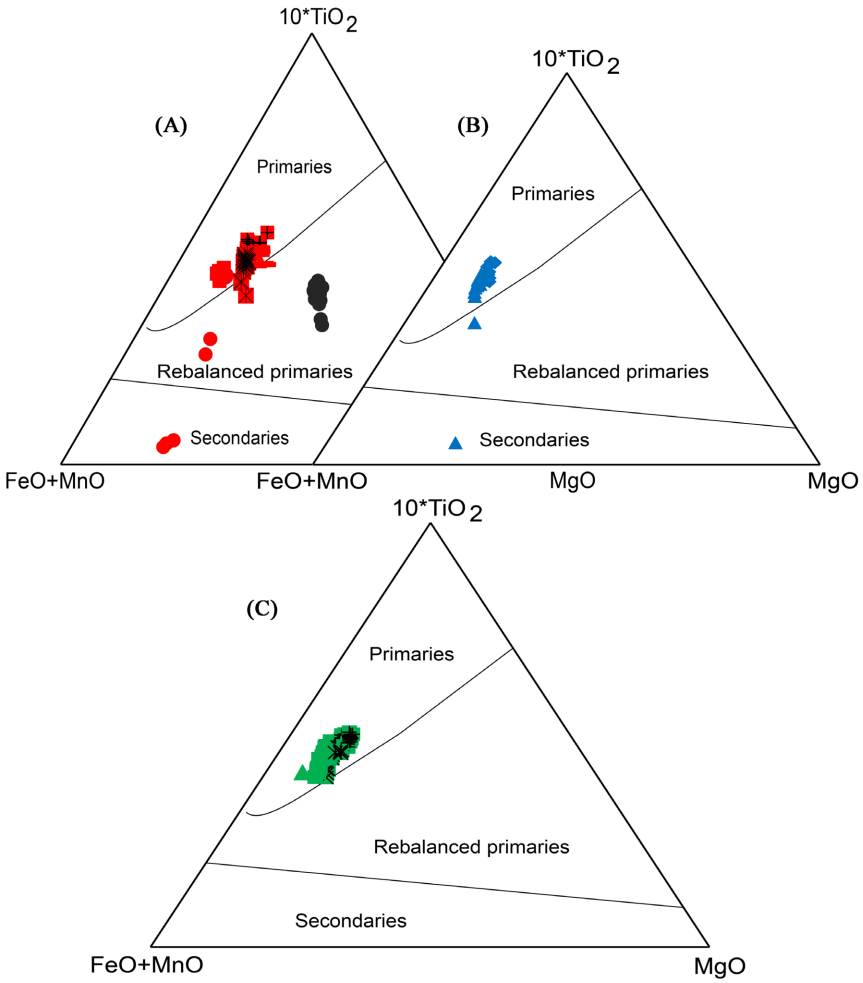

Figure 4. Domain of primary, transformed and/or neoformed biotites in the triangular diagram [(FeO + MnO)-10TiO₂-MgO] of [26]. (A) G3, (B) G2 et (C) G3. The legend is the same as that of **Figure 2**.

In the diagram by [22], the micas from the different granite massifs fall into the field of Fe-enriched biotites (**Figure 3(A)**), but with variations in distinct compositions.

5. Discussion

The different geochemical variations observed in the geochemical analyzes of the micas show that the granites of the Issia region could come from different sources. We can see that the FeO, MgO and TiO_2 contents of the muscovites in the granites decrease from G1 granites, G2 granites to G3 granites, without direct correlation between the different groups.

The projection of the analysis points of dioctahedral micas (white micas) on the binary diagram R3 + as a function of Fe + Mg + Ti + (Si-3) of [18] (**Figure 2(A)** & **Figure 2(B)**) allowed us to observe a Tschermak substitution or phengitic substitution (Al + Al ↔ Fe, Mg + Si) of the muscovites of the Issia granitoids. This Celadonite or Tschermakitic substitution can be defined as $R^{3+} + Al^{IV}$

= Si + R^{2+} (R^{3+} = Al, Fe^{3+} and R^{2+} = Mg, Fe^{2+}, Mn).

This substitution depends on temperature and pressure. Relatively high pressure and low temperature have been shown to promote an increase in the phengitic component in muscovite [27]. [28] propose, based on thermodynamic considerations, that celadonitic muscovite is more stable than pure muscovite at a higher temperature. These diagrams also show that the most phengitic muscovites are those of the G1 and G2 granites. We can also see that the muscovites which tend more towards the pure muscovite pole are those of the G3 granites and pegmatites (**Figure 2(C)**), which would therefore mean that these muscovites were formed at lower temperatures than those of the G1 and G2 granites.

The progressive enrichment in Na of muscovites from granites G3 to pegmatite IS01 (pegmatite outside granite) passing through the muscovites of intragranite pegmatites, suggests an evolution of granitic fluid towards a pegmatitic fluid. This evolution would be put in place by a fractional crystallization of the source magma, with pegmatite IS01 representing the most evolved stage. The transition of the micas of granites to pegmatites, as observed in the binary diagram of [22] (**Figure 3(B)**), from the muscovite pole to the zinnwaldite pole via Li-muscovite and Li-phengite, shows an enrichment of the source magma in Li and other incompatible elements.

As shown by the work of [15] using whole rock geochemistry, the biotites of the G3 granites display characteristics of peraluminous magma of metasedimentary origin (S-type granite). In contrast, the biotites of the G2 granites exhibit characteristics of calc-alkaline magmas. The biotites of the G1 granites are distributed within the fields of both calcalkaline and peraluminous magmas, indicating a mixed origin (I- and S-type), as demonstrated in the geochemistry section by [15].

6. Conclusions

Chemical analyzes on the mineral phases were carried out on dioctahedral (muscovite) and trioctahedral micas. For dioctahedral micas, it should be noted that the muscovites in the G1 and G2 granites have the particularity of being richer in Fe but poorer in Na than the G3 granites. Different substitution diagrams showed that most of the muscovites have undergone phengitic substitution and that the muscovites which approach the pure muscovite pole are those in G3 granites and pegmatites. All analyzed muscovites show characteristics of being either magmatic (primary muscovites) or late magmatic (secondary muscovites). With the exception of the granodiorite biotites (DAL06), which showed phlogopite characteristics, all the granite biotites are located between the siderophyllite-annite poles and are rich in Fe (Fe-biotites) and Al. However, the biotites G1 granites are less ferrous than those of G2 and G3 granites. The study of biotites has shown that the G3 granites are peraluminous and of type S, whereas the G2 and G1 granites display the characteristics of granites originating from magma of mixed origin (calcalkaline and peraluminous), thus classified as both type S

and I. Although the majority of the biotites studied present the primary characteristics, we also observe some re-equilibrated primary biotites and secondary biotites.

In perspective to this, since rare metal granites and pegmatites are very important rocks economically because they can be extremely enriched in some rare elements such as Li, Ta, Sn, Nb, Be and Cs, which are essential for the development of high-tech industries; it would be interesting to study these elements which can be enriched in micas.

Acknowledgements

This work was supported by the project T2GEM (Technologies Géophysiques et Géochemiques pour l'Exploration Minière). We thank the French Institute for Research and Development (IRD) for supporting D. Baratoux's and M. Van Lichtervelde's visits to UFHB between 2015 and 2022. We also thank Philippe De Parseval and Thierry Aigouy for for their assistance with the SEM and microprobe data acquisition at Géosciences Environnement Toulouse (GET) and Castaing Center.

Conflicts of Interest

The authors declare no conflicts of interest regarding the publication of this paper.

References

[1] Murray, R.J. (1960) The Geology of the "Zuarugu" 1/2 Fields. *Ghana Geological Survey Bulletin*, **25**.

[2] Tagini, B. (1960) Hypothèses nouvelles pour une esquisse structurale du Sud-Est de la Côted'Ivoire. DGPM.

[3] Arnould, M. (1961) Etude géologiques des migmatites et granites précambriens du Nord de la Côte-d'Ivoire et de la Haute-Volta méridionale. Mémoire BRGM.

[4] Bessoles, B. (1977) Géologie de l'Afrique: Le Craton Ouest Africain. BRGM.

[5] Lemoine, S. (1988) Evolution géologique de la région de Dabakala (NE de la Cote d'Ivoire) au Protérozoique. Possibilités d'extension au reste de la Cote-d'Ivoire et au Burkina Faso: Similitudes et différences; les linéaments de Greenville Ferkessédougou et Grand Cess-Niakaramandougou. Ph.D. Thesis. Université Clermont Auvergne, Clermont-Ferrand.

[6] Yobou, R. (1993) Pétrologie des granitoïdes du protérozoïque du centre-nord de la Côte d'Ivoire (Ferkessédougou-Marabadiassa): Évolution magmatique et contexte géodynamique. Master's Thesis, Université Paris-Sud.

[7] Doumbia, S. (1997) Géochimie, géochronologie et géologie structurale des formations birimiennes de la région de Katiola-Marabadiassa (Centre-Nord de la Côte d'Ivoire. Master's Thesis, Université d'Orléans.

[8] Feybesse, J.L., Milési, J.P., Johan, V., Dommanget, A., Calvez, J.Y., Boher, M. and Abouchami, W. (1989) La limite Archéen-Protérozoïque inférieur d'Afrique de l'Ouest: Une zone de chevauchement majeure antérieure à l'accident de Sassandra; l'exemple des régions d'Odienné et de Touba (Côte-d'Ivoire). *Compte Rendu Aca-*

démie Sciences Paris, **309**, 1847-1853.

[9] Hottin, G. and Ouédraogo, O.F. (1975) Notice explicative de la carte géologique de la République de Haute Volta à 1/1000000. Géol. des Mines, Ouagadougou.

[10] Caen-Vachette, M. (1986) Apport de la géochronologie isotopique à la connaissance du Protérozoïque Inférieur de l'Afrique de l'Ouest. Publication CIFEG 1986/10. Les formations birimiennes en Afrique de l'Ouest, 17-23.

[11] Tempier, P. (1987) Les granites de "Type Bondoukou", leur signification et leur répartition dans l'Ouest African. Lyon, Section des Sciences, 317-328.

[12] Boher, M., Abouchami, W., Michard, A., Albarede, F. and Arndt, N.T. (1992) Crustal Growth in West Africa at 2.1 Ga. *Journal of Geophysical Research*: *Solid Earth*, **97**, 345-369. https://doi.org/10.1029/91jb01640

[13] Kouamelan, A.N. (1996) Géochronologie et géochimie des formations Archéennes et Protérozoïques de la dorsale de Man en Côte d'Ivoire. Implications pour la transition Archéen-Protérozoïque. Université de Rennes 1.

[14] Koh, J.S. and Yun, S.H. (1999) The Compositions of Biotite and Muscovite in the Yuksipryong Two-Mica Granite and Its Petrological Meaning. *Geosciences Journal*, **3**, 77-86. https://doi.org/10.1007/bf02914263

[15] Brou, J.K., Van Lichtervelde, M., Kouamelan, N.A., Baratoux, D. and Thébaud, N. (2022) Petrogenetic Relationships between Peraluminous Granites and Li-Cs-Ta Rich Pegmatites in South Issia Zone (central-West of Côte D'ivoire): Petrography, Mineralogy, Geochemistry and Zircon U-Pb Geochronology. *Mineralogy and Petrology*, **116**, 443-471. https://doi.org/10.1007/s00710-022-00790-2

[16] Allou, A.B., Lu, H.Z, Guha, J., Naho, J., Carignan, J., Pothin, K. and Yobou, R. (2005) Une Correlation Genetique entre les Roches Granitiques, et les Depots Eluvionnaires, Colluvionnaires et Alluvionnaires de Columbo-Tantalite d'Issia, Centre-Ouest de la Cote d'Ivoire. *Exploration and Mining Geology*, **14**, 61-77. https://doi.org/10.2113/gsemg.14.1-4.61

[17] Joseph, B.K., Nicaise, K.A., Roland, K.B. and Yacouba, C. (2021) Pétrographie et géochimie des granitoïdes d'Issia (Centre-Ouest de la Côte d'Ivoire). *European Scientific Journal ESJ*, **17**, 287-305. https://doi.org/10.19044/esj.2021.v17n17p287

[18] Guidotti, C.V. (1984) 10. Micas in Metamorphic Rocks. In: Bailey, S.W., Ed., *Micas*, De Gruyter, 357-468. https://doi.org/10.1515/9781501508820-014

[19] Vidal, O. and Parra, T. (2000) Exhumation Paths of High-Pressure Metapelites Obtained from Local Equilibria for Chlorite-Phengite Assemblages. *Geological Journal*, **35**, 139-161. https://doi.org/10.1002/gj.856

[20] Foster, M.D. (1960) Interpretation of the Composition of Trioctahedral Micas. Geological Survey Professional Paper 354-B.

[21] Miller, C.F., Sttodart, E.F., Bradfish, L.J. and Dollase, W. (1981) Composition of Plutonic Muscovite: Genetic Implications. *Canadian Mineral*, **19**, 25-34.

[22] Tischendorf, G., Gottesmann, B., Förster, H. and Trumbull, R.B. (1997) On Li-Bearing Micas: Estimating Li from Electron Microprobe Analyses and an Improved Diagram for Graphical Representation. *Mineralogical Magazine*, **61**, 809-834. https://doi.org/10.1180/minmag.1997.061.409.05

[23] Abdel-Rahman, A.M. (1996) Discussion on the Comment on Nature of Biotites in Alkaline, Calc-Alkaline and Peraluminous Magmas. *Journal of Petrology*, **37**, 1031-1035. https://doi.org/10.1093/petrology/37.5.1031

[24] Abdel-Rahman, A.M. (1994) Nature of Biotites from Alkaline, Calc-Alkaline, and Peraluminous Magmas. *Journal of Petrology*, **35**, 525-541. https://doi.org/10.1093/petrology/35.2.525

[25] Nachit, H., Razafimahefa, N., Stussi, J.M. and Carron, J.P. (1985) Composition chimique des biotites et typologie magmatique des granitoids. *Comptes Rendus Hebdoma-daires de l'Académie des Sciences*, **301**, 813-818.

[26] Nachit, H., Ibhi, A., Abia, E.H. and Ben Ohoud, M. (2005) Discrimination between Primary Magmatic Biotites, Reequilibrated Biotites and Neoformed Biotites. *Comptes Rendus. Géoscience*, **337**, 1415-1420. https://doi.org/10.1016/j.crte.2005.09.002

[27] Velde, B. (1967) Si^{4+} Content of Natural Phengites. *Contributions to Mineralogy and Petrology*, **14**, 250-258. https://doi.org/10.1007/bf00376643

[28] Anderson, J.L. and Rowley, M.C. (1981) Synkinematic Intrusion of Peraluminous and Associated Metaluminous Granitic Magma, Whipple Mountains, California. *Contributions to Mineralogy and Petrology*, **19**, 83-101.